Supplementary materials:

Helical Luttinger liquid on the edge of a 2-dimensional topological antiferromagnet

The supplementary information file contains seven sections:

Contents

1. Optic images of device #1

The optic images of device #1 taken before different thermal cycles, are displayed in **Figure S1**. The images show the evolution of the Hall bar device #1. By transport measurement on device #1, we obtain the results including the magnetic field dependence of bulk resistance in Fig. 1, the V_g dependence of R_{xx} in Fig. 2 and edge conduction in Fig. 4 (except for Fig. 4f) in the main text.

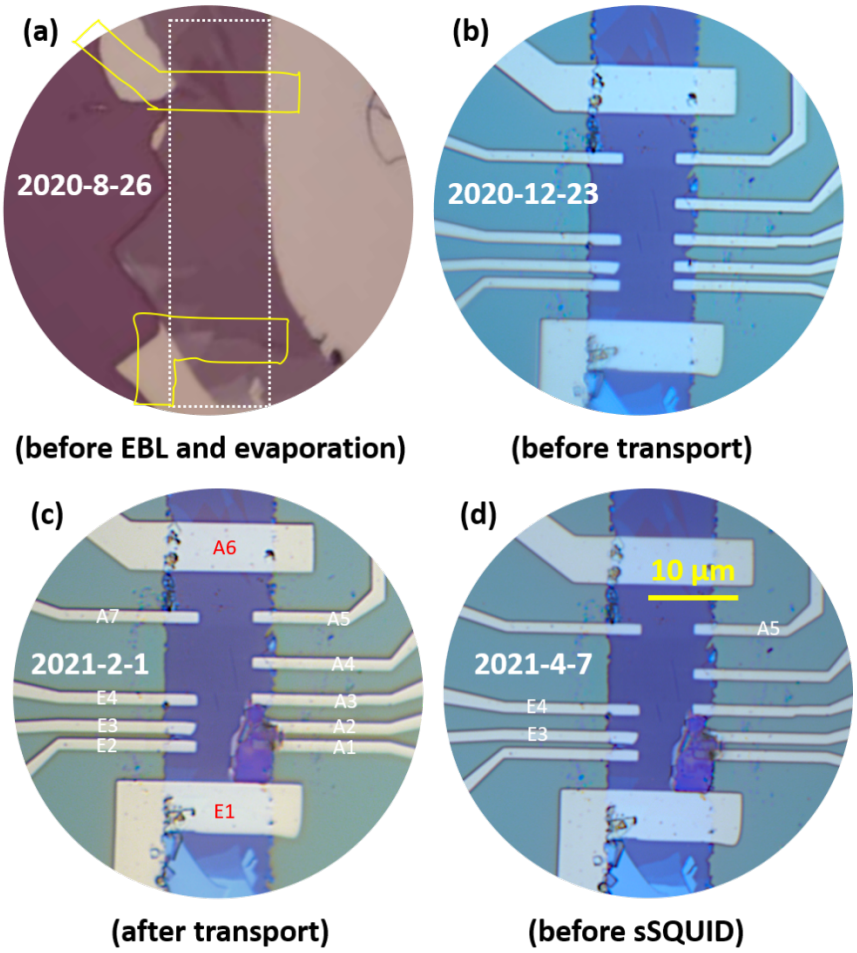

Figure S1 | Optic images of the Hall bar device made from the 6-SL $MnBi_2Te_4$ flake. **(a)** Before EBL, the image of the flake with several different thicknesses on SiO_2/Si substrate. The image is taken soon after the flake exfoliated from single crystal of $MnBi_2Te_4$. The white dotted line indicates the contour after manually scratching. The yellow solid line indicates the contour of the gold contact made by EBL and thermal evaporation. **(b)** Before transport measurement, the image shows the Hall bar device. Through the first thermal cycle, we obtained the magnetic field dependence of bulk resistance in Fig. 1, the V_g dependence of ρ_{xx} in Figure 2 and edge conduction in Figure 4 in the main text. **(c)** After transport measurement, the image shows the Hall bar device with broken area in the bottom left corner. The area around electrode A1 and electrode A2 are damaged (A and B in the main text). It is possibly caused by the Electro-Static discharge (ESD), give rise to a sudden large current flowing through this area during the measurement. **(d)** Before scanning SQUID measurement, the image of the Hall bar device seems the same with that in (c), so electrode of E3, E4, A5 instead of E2, A3, A4, are chosen for current density measurement, to avoid the effects from burned area around A1A2 as far as possible.

As shown in Figure S1(c), after transport measurement, the area around electrode A1 and A2 (electrode A and B in the main text) are broken with some burned-up process, possibly due to ESD process (a sudden large current flowing through this area) during the transport measurement.

For the current flux measurement in the sSQUID microscope (for example, the

current flowing from A5 to E4, equivalent to C and H in the main text), the bulk and the edges can be treated as uncoupled parallel resistors, which can be calculated by dividing R_{2T} by the respective current percentage [1]. Here, during the scanning, the lowest $R_{2T} > 150k\Omega \gg h/e^2$ reveals the fact that the edge channels are not ballistic. If the edge transport is in diffusive regime, the ratio of upper and lower edges (from A5 to E4) is expected to range from 1:1 to 1:2 based on the path lengths. However, before scanning measurement, as shown in Figure S1(c) and (d) the lower edge is broken, especially between A1 and A2 area. The burned area affects the distribution between upper and lower edges, since the lower edge crossing A1 and A2 is interrupted. Such inhomogeneity is revealed in the reconstructed current density in Figure 2(e) and (f) in the main text.

2. Calibration of sample #1

Figure S2 shows the magnetic field dependent Hall resistivity ρ_{yx} taken with a +25 V gate voltage. The probes are labeled in the inset of Figure S2. No obvious hysteresis behavior is observed during the magnetic field sweeping. Although the data in the measured ρ_{yx} around zero magnetic field is not absolute zero, the overall trend is consistent with the fact that the $MnBi_2Te_4$ is a tetradymite compound which consists of Te-Bi-Te-Mn-Te-Bi-Te septuple layers (SLs) stacking in the vertical direction, and the spins of Mn within each SL couple ferromagnetically with an out-of-plane easy axis, while spins in adjacent SLs couple antiferromagnetically forming an A-type antiferromagnetism (AFM). The zero Hall plateau shown in Figure S2 is consistent with the previous report [2] as a signature of the existence of axion insulator. The quantized h/e^2 plateaus at high fields are consistent with the characteristic features of the Chern insulator phase where a conductive edge encloses an insulating bulk. The phase transition between Chern insulator and axion insulator [3,4] is labeled by the black and red arrows in Figure S2a.

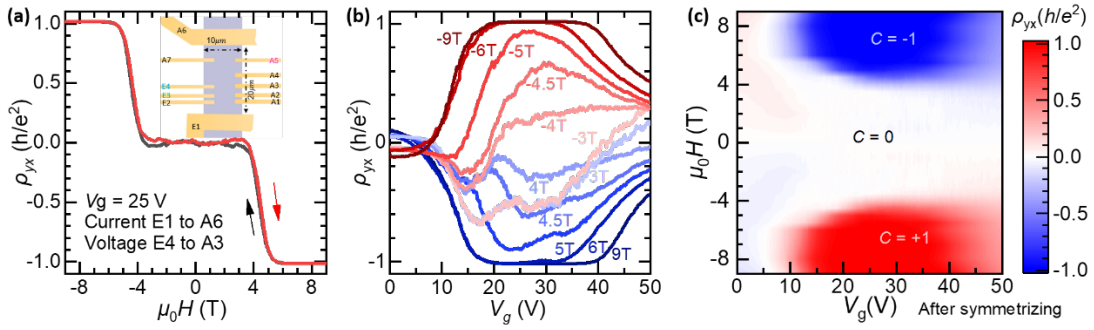

Figure S2 | Gate dependent Hall resistivity of device #1. (a) magnetic field dependence of ρ_{yx} at $V_g = 25$ V. The resistance is caculated from voltage drop between probe A3 and E4, divided by current flow from E1 to A6. **(b)** electric field dependence of ρ_{yx} at different magnetic field μH at $T = 1.8$ K. When E_F lies within the surface band gap for $20 < V_g < 40$ V, the quantized Hall plateau at high μH are key signatures of the Chern insulator state. **(c)** Experimental phase diagram obtained by a colored contour plot of the ρ_{yx} value adapted from the data in (b) at different gate voltage V_g and magnetic field μH. In the phase diagram Chern insulator phase ($C = \pm 1$) and zero Hall plateau phase ($C = 0$) are clearly visualized.

As shown in the field-gate diagram in Figure S2 (c), the value of ρ_{yx} remains zero in the field range from -3.5 T to 3.5 T, forming a zero Hall plateau. As the μH field goes up, ρ_{yx} increases steeply and quickly approaches to a quantized Hall plateau above 6 T, confirming a phase transition to a Chern insulator.

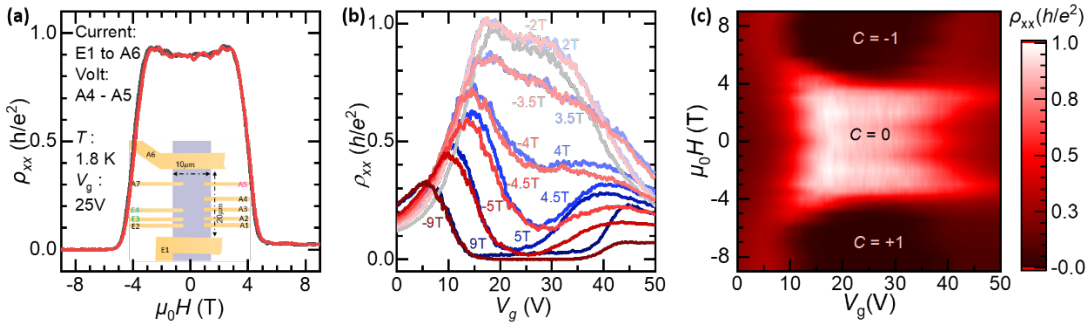

Figure S3 | Gate dependent longitudinal resistivity of device #1. (a) magnetic field dependence of ρ_{xx} at $V_g = 25$ V. The resistance is caculated from voltage drop between probe A4 and A5, divided by current flow from E1 to A6. **(b)** electric field dependence of ρ_{xx} at selected magnetic fields at $T = 1.8$ K. The relatively high resistivity is obtained within $15 < V_g < 35$ V. **(c)** Experimental phase diagram obtained by a colored contour plot of the ρ_{xx} value adapted from the data in (b) at different gate voltage V_g and magnetic field μH. The Chern number are labeled in the diagram.

3. bulk resistance of device #1

To confirm the transition of the bulk, corresponding to the transition of the edge state as revealed by the gate voltage map in Figure S2 and Figure S3, we conduct a global transport measurement of device shown in Figure S1. As indicated in ref [5], the ideal geometry for true bulk resistance without any edge channels is the Corbino disk, however, for a quantized Hall device with high quality, we might bypass the contribution of edge channel by ground all floating probes. As shown in the inset of Figure S4, we run a current through a pair of electrodes (C and H in the main text) on opposite site of the device while grounding all other electrodes. By this way, current mainly goes through the bulk which allows us to only probe the bulk resistance.

It is also worth mentioning that, for multi-terminal devices, contacts were made by Cr/Au thermal evaporation. The lock-in measured (200nA) two-terminal resistance between A3 and E4 as indicated in the inset of **Figure S4** (C and H in the main text) at $T = 1.8$ K, $\mu_0 H = 9$T and $V_g = 25$V (at quantized regime ρ_{yx} is ideally to be 25812 ohms) is about 26 kiloohms, so the contact resistance is about 190 ohms. We have measured all the combination of eleven contacts and the results are in close values (<200ohm).

The curves in **Figure S4** shows such a magnetic field dependent bulk resistance measurement taken at different temperatures. It reveals two MITs with a metallic state separating two insulating states at two ends.

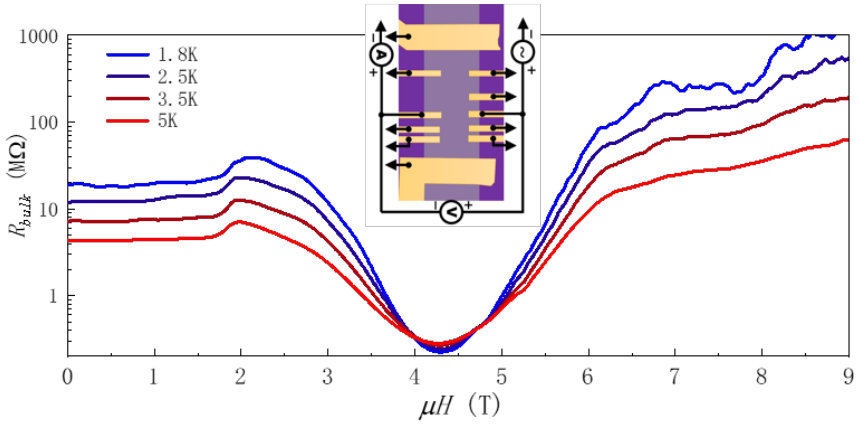

Figure S4 | The magnetic field dependence of bulk resistance. The data are obtained from 0 T to 9 T at different temperature from 1.8 K to 5 K. Inset: schematic diagram of setup for bulk resistance measurement.

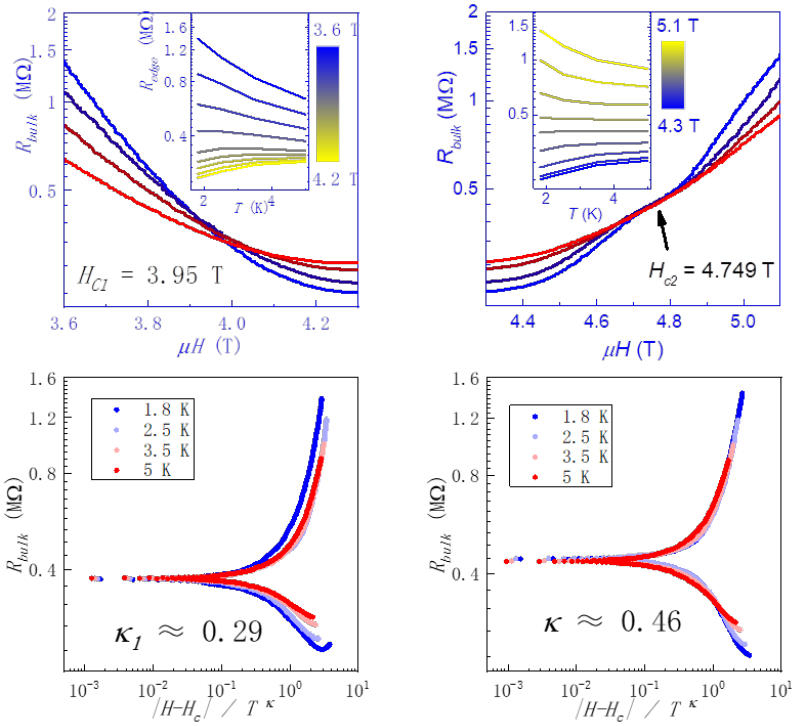

Figure S5 | Two metal-insulator-transitions (MITs) in magnetic sweeping. (a) The first transition from insulator to metal around the cross point at $H_{C1} = 3.95$ T, **(b)** the second transition from metal to insulator transition around cross point $H_{C2} = 4.749$ T. The bulk resistance magnitude maintains several mega Ohms at both zero field and high field regime. This is much larger than the order of R_{xx}, indicating a non-negligible contribution from edge channel. The inset in (b) and (c) are temperature dependence of R_{bulk} at different μH. **(c)(d)** the scaling analysis of plotting all the curves of R_{bulk} as a function of $|H - H_C|$ over T^{κ} around H_{C1} and H_{C2} giving the index $\kappa_1 = 0.29$ and $\kappa_2 = 0.46$ respectively.

Figure S5 (a) and (c) are zoom-in plots of such transition. The first one is an insulator to metal transition at around 3.95 T, while the second one is a metal to insulator transition at around 4.75 T.

To gain quantitative insight into these MITs, we perform a scaling analysis of R_{bulk} with respect to T and H in the vicinity of H_c as $R_{bulk} \propto (H - H_c)/T^{\kappa}$ (**Figure S5**). For

the first MIT at $H_{c1} = 3.95\text{T}$, $\kappa_1 = 0.29$. For the second MIT at $H_{c2} = 4.75\text{T}$, $\kappa_2 = 0.46$. We note that $\kappa_2 = 0.46$ at higher field is close to that in the delocalization process during the (QH) plateau transition [6–9]. On the other hand, $\kappa_1 = 0.29$ suggests the MIT at lower field may be related to the magnetic disorders [10,11] known to exist in $MnBi_2Te_4$, especially in its AFM state.

Value	Type of transition
$\kappa = 0.42$	between the lowest two Landau levels [6]
$\kappa = 0.42$	for transition between $\nu = 1/2$ and $2/5$ plateau [7]
$\kappa = 0.45$	from quantum Hall liquid to quantum Hall insulator [8]
$\kappa = 0.43$	Disorder induced transition between quantum Hall insulator to quantum Hall liquid tuned by carrier concentration [9]

Table S1 | Some critical component of phase transitions in quantum Hall system.

One important conclusion from the analysis on bulk resistance is that the zero-field insulator is topologically distinct from the Chern insulator as they are bridged by a metallic state in between where the bandgap closes and re-opens. More precisely, they have different topological indices, that $C = 0$ for the zero-field insulator with ZHP, and $C = 1$ for the Chern insulator at high field.

4. Current flow into different probes of device #1

In the edge dominated regime, the current resolved scanning SQUID measurements are performed on the 6-SL device, to further detect the edge conduction in the zero Hall plateau state.

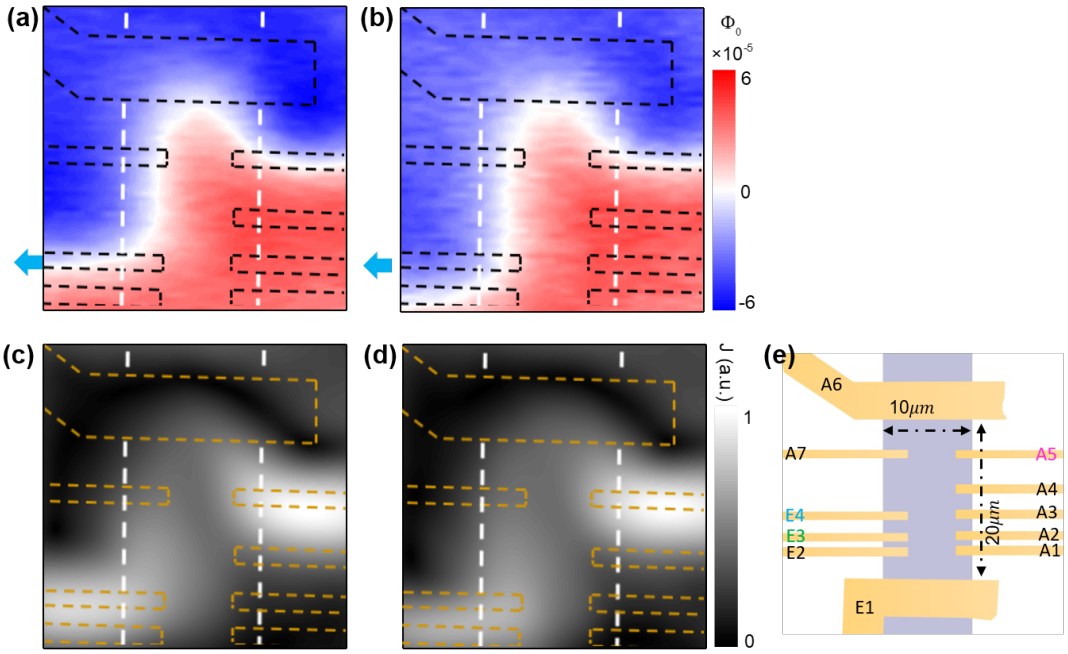

Figure S6 | Flux and current maps of the multi-terminal Hall bar device at best tuned gate voltage. **(a)** current flux with current flowing from A5 to E4 **(b)** current flux with current flowing from A5 to E3. **(c)** current map with reconstructed 2D current density calculated from the data in (a). **(d)** current density calculated from the data in (b). The dashed lines in map indicate the approximate geometry of the sample. Scale bar shown in the map indicates 5μm. **(e)** schematic diagram of the Hall bar device.

5. HLL behavior in device #1

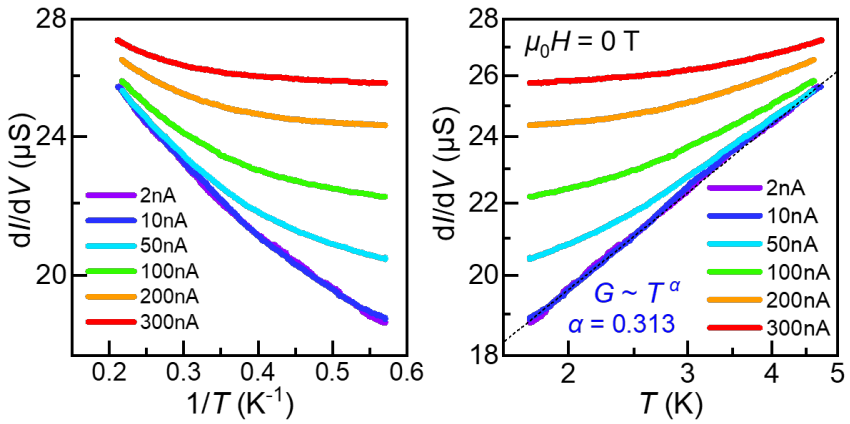

Figure S7 | Relation between differential conductance and temperature. (a) differential conductance $G = dI/dV$ as a function of $1/T$. All the curves show curvature. It clearly indicates that a simple thermal activated process is not appropriate for the edge conduction. (b) G as a function of T in double log scale.

As mentioned in the main text, there are three possible origins for the helical edge states at $\mu_0 H = 0$. The first possibility is the side surface described by the single nondegenerate Fermi arc, with specific termination protected by the PT symmetry [3] as shown in Fig. 1a. Such surface state is essentially half of an ordinary 2D electron gas

(2DEG) because it violates the fermion doubling theorem [12]. Meanwhile, the other half of 2DEG exists on the opposite side surface. With reducing thickness, the half 2DEG with massless dispersion will evolve into a helical 1D channel. However, there is a bandgap ~ 0.047 eV due to quantum confinement on the side surface of 6-SL flake [3]. The helical 1D channel with such a large gap is hard to affect transport with low energy excitation. The second possibility is the 1D helical edge induced by the hybridization of top and bottom surfaces in an AFM phase as illustrated in Fig. 4d. The helical edge has a tiny gap due to the translation-symmetry breaking in the z direction according to model calculations [13]. In presence of disorder, the quasiparticle spectrum is broadened and the edge gap is reduced. Furthermore, the 1D helical edge state is dissipative because backscattering by disorder is allowed with TRS breaking. The third possible origin comes from the surface Hall effect [15,16] in axion phase of MBT, which can be viewed as a pair of chiral hinge modes with opposite propagating directions [17,18]. However, in simulation [17] the necessary number of SLs (n_z) to observe half quantized chiral currents is about 100, much larger than $n_z = 6$ for our device.

Although the three possible origins share the same topological nature protected by the PT symmetry, we argue that the gapped 1D helical edge state is most reasonable for the even-layer thin film device. We illustrate the band structure of topological phase and bulk-boundary correspondence as a function of $\mu_0 H$ applicable to the even-layer, as introduced in the main text. At the AFM ground state, the two top and two bottom surface bands are already inverted due to the strong spin orbit coupling. Since the surface magnetization is quite small [19], the inverted bands with even and odd parity opens a hybridization gap. Two pairs of hybridization bands give rise to a pair of helical edges. Interactions are allowed between two branches of helical edge states to create electron-hole pairs, which can be regarded as bosons. Unlike the Fermi liquid and the chiral 1D liquid, due to the reduced dimensionality and TRS breaking, the bandgap and internal backscattering is unavoidable, giving rise to a helical Luttinger (HLL) liquid [20], which is a strongly correlated system.

6. Calibration of device #2

In order to reveal the evolution of interaction within the edge from the helical Luttinger liquid regime at zero magnetic field to the chiral Fermi liquid regime in the presence of external magnetic field dependent, we take the measurement on device #2 made from another 6SL $MnBi_2Te_4$ flake.

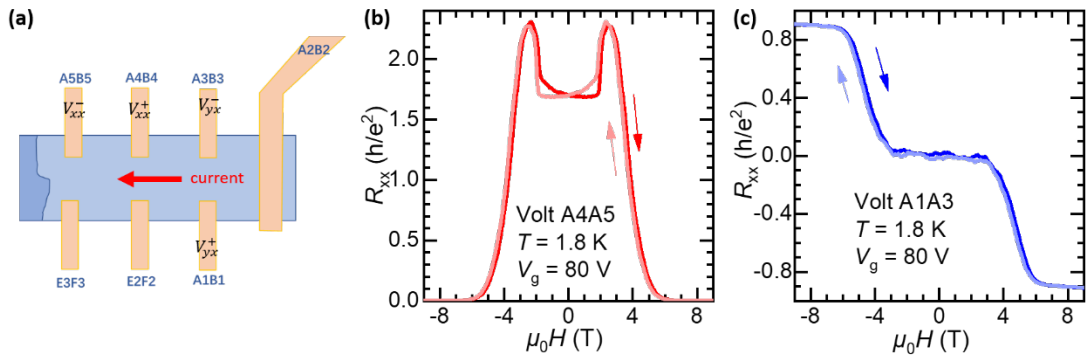

Figure S8 | Magnetic field dependent transport properties of device #2. (a) schematic diagram of device #2. The direction of current flow is indicated by the red arrow. Voltage probes selected for longitudinal resistance and Hall resistance is labeled by V_{xx}^{+}, V_{xx}^{-} and V_{yx}^{+}, V_{yx}^{-} respectively. (b) magnetic field dependent longitudinal resistance. (c) magnetic field dependent Hall resistance. At 9T the Hall signal is about $0.9h/e^2$.

Overall, the Chern insulator features of Chern insulator at high field is observed in the nearly quantized Hall resistance associated with vanishing longitudinal resistance. However, the sample quality of device #2 is not that good as that of device #1. First, the best tuned gate voltage (80V) is much larger than that of device #1. Second, the Hall resistance at 9T is about $0.9h/e^2$. This is possibly because the bulk is not insulating enough and not all carriers in the bulk are localized.

7. HLL behavior in device #2

We present experimental results on the edge conduction in the presence of external field. While the system is in zero Hall plateau regime, we observe the onset of a nonlinear current-voltage characteristic, consistent with a non-Fermi liquid behavior, such as a Luttinger liquid ($\alpha \approx 0.4$). When the system exhibits typical Chern insulator features, we observe the Ohmic tunneling resistance between the terminals, typical for a Fermi liquid ($\alpha \approx 0$).

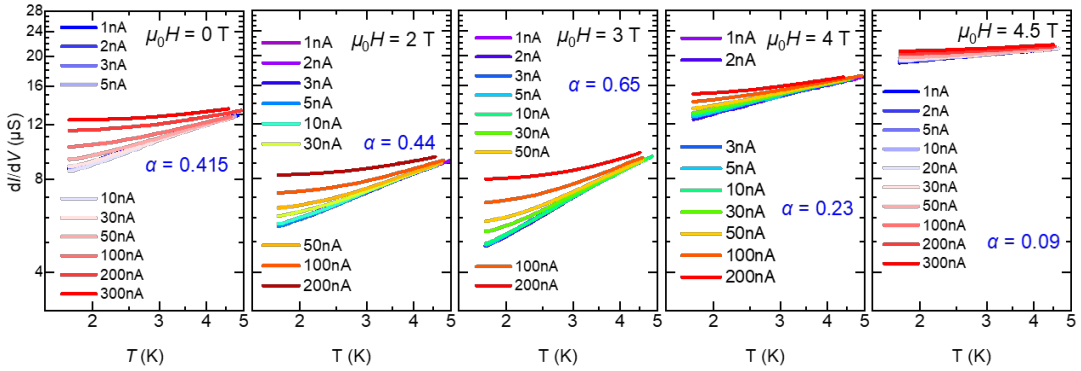

Figure S9 | **Excitation dependence of the edge conductance G.** The excitations are from I_{AC} = 1 nA to 300 nA at different T. The log-log plot indicates a power-law behavior is not universal and depends on external magnetic field.

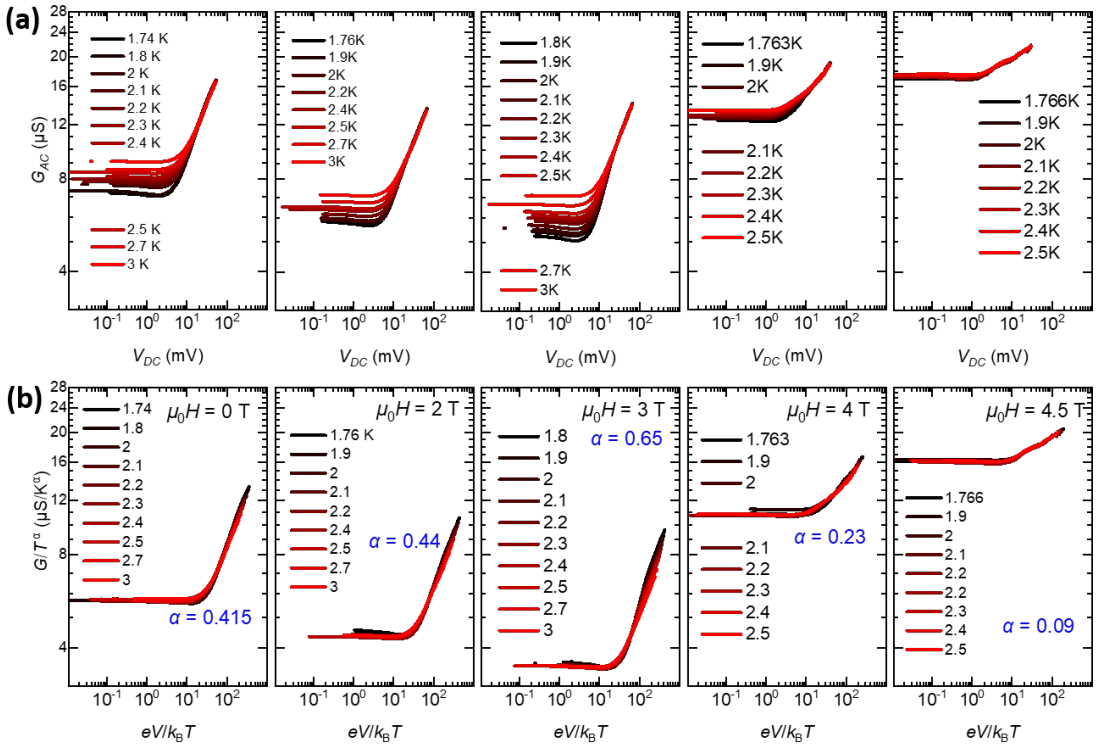

Figure S10 | Bias voltage dependence of edge differential conductance at different magnetic fields. (a) The panels in the upper row shows V_{DC} dependence of the edge differential conductance dI/dV at different fields. Data are measured from T below 1.8 K up to 5.5 K, with the ac modulation current $I = 2$ nA. (b) The panels in the lower row shows the illustration of all the measured data points except the saturation region collapse onto a single curve by scaling the measured dI/dV. The component α is listed in each panel, and the summary of α as a function of $\mu_0 H$ is shown in the main text.

Factors that affect the HLL are complicated. Similar result has also been observed in heterostructure of InAs/GaSb [21]. In a helical edge state, such deviations of conductance from the quantized value [22,23] has been attributed to the trivial impurities interacting with the edge electrons, such as bulk electrons trapped by potential inhomogeneities [24,25], defect of crystalline, Rashba spin-orbit coupling [26,27] and so on. In our experiment, for device #1 at zero field $\alpha \approx 0.3$, while for device #2 $\alpha \approx 0.4$. This observation shows that, the Luttinger liquid exponent is not a universal but depends on sample parameters.

8. Reference

[1] K. C. Nowack, E. M. Spanton, M. Baenninger, M. König, J. R. Kirtley, B. Kalisky, C. Ames, P. Leubner, C. Brüne, H. Buhmann, L. W. Molenkamp, D. Goldhaber-Gordon, and K. A. Moler, *Imaging Currents in HgTe Quantum Wells in the Quantum Spin Hall Regime*, Nat. Mater. **12**, 787 (2013).

[2] C. Liu, Y. Wang, H. Li, Y. Wu, Y. Li, J. Li, K. He, Y. Xu, J. Zhang, and Y. Wang, *Robust Axion Insulator and Chern Insulator Phases in a Two-Dimensional Antiferromagnetic Topological Insulator*, Nat. Mater. **19**, 5 (2020).

[3] J. Li, Y. Li, S. Du, Z. Wang, B.-L. Gu, S.-C. Zhang, K. He, W. Duan, and Y. Xu, *Intrinsic Magnetic Topological Insulators in van Der Waals Layered MnBi2Te4-Family Materials*, Sci. Adv. **5**, eaaw5685 (2019).

[4] D. Zhang, M. Shi, T. Zhu, D. Xing, H. Zhang, and J. Wang, *Topological Axion States in the Magnetic Insulator $MnBi_2Te_4$ with the Quantized Magnetoelectric Effect*, Phys. Rev. Lett. **122**, 206401 (2019).

[5] D. Ovchinnikov, X. Huang, Z. Lin, Z. Fei, J. Cai, T. Song, M. He, Q. Jiang, C. Wang, H. Li, Y. Wang, Y. Wu, D. Xiao, J.-H. Chu, J. Yan, C.-Z. Chang, Y.-T. Cui, and X. Xu, *Intertwined Topological and Magnetic Orders in Atomically Thin Chern Insulator MnBi2Te4*, Nano Lett. **21**, 2544 (2021).

[6] H. P. Wei, D. C. Tsui, M. A. Paalanen, and A. M. M. Pruisken, *Experiments on Delocalization and University in the Integral Quantum Hall Effect*, Phys. Rev. Lett. **61**, 1294 (1988).

[7] L. Engel, H. P. Wei, D. C. Tsui, and M. Shayegan, *Critical Exponent in the Fractional Quantum Hall Effect*, Surf. Sci. **229**, 13 (1990).

[8] W. Pan, D. Shahar, D. C. Tsui, H. P. Wei, and M. Razeghi, *Quantum Hall Liquid-to-Insulator Transition in In 1-x Ga x As/InP Heterostructures*, Phys. Rev. B **55**, 15431 (1997).

[9] L. W. Wong, H. W. Jiang, N. Trivedi, and E. Palm, *Disorder-Tuned Transition between a Quantum Hall Liquid and Hall Insulator*, Phys. Rev. B **51**, 18033 (1995).

[10] C.-Z. Chang, W. Zhao, J. Li, J. K. Jain, C. Liu, J. S. Moodera, and M. H. W. Chan, *Observation of the Quantum Anomalous Hall Insulator to Anderson Insulator Quantum Phase Transition and Its Scaling Behavior*, Phys. Rev. Lett. **117**, 126802 (2016).

[11] C. Liu, Y. Ou, Y. Feng, G. Jiang, W. Wu, S. Li, Z. Cheng, K. He, X. Ma, Q. Xue, and Y. Wang, *Distinct Quantum Anomalous Hall Ground States Induced by Magnetic Disorders*, Phys. Rev. X **10**, 041063 (2020).

[12] H. B. Nielsen and M. Ninomiya, *The Adler-Bell-Jackiw Anomaly and Weyl Fermions in a Crystal*, Phys. Lett. B **130**, 389 (1983).

[13] W. Lin, Y. Feng, Y. Wang, Z. Lian, H. Li, Y. Wu, C. Liu, Y. Wang, J. Zhang, Y. Wang, X. Zhou, and J. Shen, *Direct Visualization of Edge State in Even-Layer $MnBi_2Te_4$ at Zero Magnetic Field*, ArXiv210510234 Cond-Mat (2021).

[14] Z. Liu, D. Qian, Y. Jiang, and J. Wang, *Dissipative Edge Transport in Disordered Axion Insulator Films*, ArXiv210906178 Cond-Mat (2021).

[15] R.-L. Chu, J. Shi, and S.-Q. Shen, *Surface Edge State and Half-Quantized Hall Conductance in Topological Insulators*, Phys. Rev. B **84**, 085312 (2011).

[16] M. Mogi, Y. Okamura, M. Kawamura, R. Yoshimi, K. Yasuda, A. Tsukazaki, K. S. Takahashi, T. Morimoto, N. Nagaosa, M. Kawasaki, Y. Takahashi, and Y. Tokura, *Experimental Signature of Parity Anomaly in Semi-Magnetic Topological Insulator*, ArXiv210504127 Cond-Mat (2021).

[17] R. Chen, S. Li, H.-P. Sun, Q. Liu, Y. Zhao, H.-Z. Lu, and X. C. Xie, *Using Nonlocal Surface Transport to Identify the Axion Insulator*, Phys. Rev. B **103**, L241409 (2021).

[18] M. Gu, J. Li, H. Sun, Y. Zhao, C. Liu, J. Liu, H. Lu, and Q. Liu, *Spectral*

Signatures of the Surface Anomalous Hall Effect in Magnetic Axion Insulators, Nat. Commun. **12**, 3524 (2021).

[19] Y. J. Chen, L. X. Xu, J. H. Li, Y. W. Li, H. Y. Wang, C. F. Zhang, H. Li, Y. Wu, A. J. Liang, C. Chen, S. W. Jung, C. Cacho, Y. H. Mao, S. Liu, M. X. Wang, Y. F. Guo, Y. Xu, Z. K. Liu, L. X. Yang, and Y. L. Chen, *Topological Electronic Structure and Its Temperature Evolution in Antiferromagnetic Topological Insulator* $MnBi_2Te_4$, Phys Rev X **9**, 041040 (2019).

[20] C. Wu, B. A. Bernevig, and S.-C. Zhang, *Helical Liquid and the Edge of Quantum Spin Hall Systems*, Phys. Rev. Lett. **96**, 106401 (2006).

[21] T. Li, P. Wang, H. Fu, L. Du, K. A. Schreiber, X. Mu, X. Liu, G. Sullivan, G. A. Csáthy, X. Lin, and R.-R. Du, *Observation of a Helical Luttinger Liquid in InAs/GaSb Quantum Spin Hall Edges*, Phys. Rev. Lett. **115**, 136804 (2015).

[22] A. Roth, C. Brüne, H. Buhmann, L. W. Molenkamp, J. Maciejko, X.-L. Qi, and S.-C. Zhang, *Nonlocal Transport in the Quantum Spin Hall State*, Science **325**, 294 (2009).

[23] L. Du, I. Knez, G. Sullivan, and R.-R. Du, *Robust Helical Edge Transport in Gated InAs/GaSb Bilayers*, Phys. Rev. Lett. **114**, 096802 (2015).

[24] J. Maciejko, C. Liu, Y. Oreg, X.-L. Qi, C. Wu, and S.-C. Zhang, *Kondo Effect in the Helical Edge Liquid of the Quantum Spin Hall State*, Phys. Rev. Lett. **102**, 256803 (2009).

[25] J. I. Väyrynen, M. Goldstein, Y. Gefen, and L. I. Glazman, *Resistance of Helical Edges Formed in a Semiconductor Heterostructure*, Phys. Rev. B **90**, 115309 (2014).

[26] F. Geissler, F. Crépin, and B. Trauzettel, *Random Rashba Spin-Orbit Coupling at the Quantum Spin Hall Edge*, Phys. Rev. B **89**, 235136 (2014).

[27] F. Crépin, J. C. Budich, F. Dolcini, P. Recher, and B. Trauzettel, *Renormalization Group Approach for the Scattering off a Single Rashba Impurity in a Helical Liquid*, Phys. Rev. B **86**, 121106 (2012).